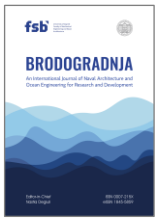
Brodogradnja Volume 78 Number 1 (2027) 78109

University of Zagreb
Faculty of Mechanical
Engineering and Naval
Architecture

journal homepage: www.brodogradnja.fsb.hr

Brodogradnja

An International Journal of Naval Architecture and
Ocean Engineering for Research and Development



Effect of carling-stiffener arrangement on the buckling and ultimate strength characteristics of a transverse bulkhead panel in FLNG: a nonlinear finite element investigation

Myung-Su Yi[1], *Da-Bin Jung*[1], *Jung-Goo Park*[2] *and Joo-Shin Park*[2,*]

[1]*Department of Naval Architecture and Ocean Engineering, Chosun University, Gwangju 61452, Republic of Korea*
[2] *Ship & Offshore Research Institute, Samsung Heavy Industries Co., Ltd., Geoje 53261, Republic of Korea*

ARTICLE INFO

Keywords:
Carling stiffener
Buckling
Ultimate strength
Nonlinear finite element analysis
Sub-modelling
Transverse bulkhead
Ship structures
Post-buckling reserve strength
Initial imperfection
Fabrication sequencing
Offset distance

ABSTRACT

Local carlings can modify elastic buckling restraint without governing the nonlinear load resistance of a stiffened bulkhead. Five arrangements in an FLNG transverse bulkhead were examined under a Design Load combining hydrostatic pressure and hull induced boundary deformation. The numerical basis was assessed using local shell sizes of 20, 50, 100 and 200 mm through linear, eigenvalue and nonlinear analyses. At 50 mm, the maximum linear displacement matched the 20 mm result at the reported precision, the first eigenvalue differed by 0.69 %, and the model used 17.2 % fewer elements. The nonlinear paths and broad deformation patterns were similar, although graphical sampling showed increasing displacement sensitivity at higher loading and local peak stress remained mesh dependent. These findings support 50 mm as a practical engineering balance for comparative panel response. Ultimate Strength was defined by the intersection of the elastic and plastic branches of each load displacement curve. Reducing three carlings to one lowered the elastic buckling factor by approximately 5.8 %, while the Ultimate Strength factor changed from 2.20 to 2.19; all five arrangements remained within 2.19 to 2.21 times Design Load. The results distinguish elastic modal restraint from nonlinear redistribution and support qualified examination of reduced carling details. Application remains specific to the investigated loading, imperfection assumptions and exclusion of welding residual stress; fabrication benefits require shop confirmation.

1. Introduction

1.1 Background and motivation

A floating liquefied natural gas (FLNG) facility integrates gas processing and liquefaction equipment on deck with cryogenic product storage in the hull. Its structural design must accommodate both a floating process plant and a marine hull. The deck and its supporting structure transfer topside loads into the hull, while bottom and side structures sustain hydrostatic and environmental demands. Longitudinal framing, girders and transverse bulkheads form interconnected load paths and define the tank and compartment arrangement. The

* Corresponding author.
E-mail address: scv7076@nate.com

https://doi.org/10.21278/brod78109
Received 24 September 2026; Received in revised form 01 November 2026; Accepted 09 November 2026
Available online 13 November 2026
ISSN 0007-215X; eISSN 1845-5859

Prelude design illustrates this integration through its double hull, double deck and centerline ballast structure, developed to reconcile topside loads, buoyancy and cargo containment requirements [1]. These particular features illustrate the broader design problem; they are not asserted to be the arrangement of every FLNG unit.

In such a structure, global hull deformation and local panel loading cannot be considered independently. A transverse bulkhead provides compartment boundaries and restraint to the surrounding hull structure, while its plating and stiffeners experience local bending and membrane action. A change to a small reinforcing member can alter the restraint of a buckling mode even when the principal load path remains nearly unchanged. Local assessment should therefore retain the deformation imposed by the surrounding hull and the pressure acting on the panel, rather than infer adequacy from an isolated detail model.

Buckling assessment identifies sensitivity to instability, whereas ultimate strength assessment examines the nonlinear resistance available as deformation and yielding redistribute load through the plate and stiffener system [2, 3]. The distinction matters because local instability need not coincide with exhaustion of the panel resistance. Conversely, a satisfactory linear stress field does not by itself establish the nonlinear margin of an imperfect structure. Evaluating both responses gives a stronger basis for selecting local reinforcement and avoiding unnecessary fabrication work while preserving the relevant structural resistance. This motivates the present comparison of carling arrangements in an FLNG transverse bulkhead.

The governing combination of depth dependent hydrostatic pressure and hull induced boundary deformation is termed the Design Load (DL) throughout this paper. Its reference level is 100 %, or load multiplier $\lambda = 1$. Both components define the common loading pattern used to compare the five arrangements.

Carlings are short members fitted locally between adjacent ordinary stiffeners. Ordinary stiffeners support the plating and span between primary supporting members, such as girders and webs; carlings and connection brackets are distinct local details. Changes in carling position and connection can accommodate fabrication access or geometric interference. This study evaluates their structural consequences rather than assuming that linear stress or elastic buckling checks alone establish equivalence. No general classification approval practice is inferred.

The specific question is whether a production motivated change in local carling restraint changes elastic buckling and Ultimate Strength by comparable amounts. The study addresses that question under one common load pattern using established numerical procedures. It does not assume that a favourable elastic result proves nonlinear equivalence, or that a carling reduction remains suitable for every loading condition.

1.2 Related work

Established treatments of plate and stiffened panel strength distinguish elastic buckling from nonlinear collapse [2, 3]. Reviews and numerical studies quantify compressive resistance and the effects of nonuniform loading and degradation [4-6]. IACS UR S35 [7] addresses buckling assessment of ship structural elements; the ABS guide [8] addresses buckling and ultimate strength of offshore structures. These references motivate appropriate structural assessment but are not cited here as prescribing the present carling modification procedure.

Much of the literature concerns plating with ordinary stiffeners spanning between primary supporting members. Carlings are local members between ordinary stiffeners, while brackets provide local connection reinforcement. The steel bracket study of Lee et al. [9] illustrates the importance of nonlinear assessment of a local detail, but does not establish the response of the carling configurations considered here.

1.3 Review of recent related studies

Several recent studies have advanced the prediction of ultimate strength for primary stiffened panels rather than for locally fitted details. Zhang et al. [10] proposed a boundary function of four key parameters to classify the failure mode of stiffened panels and derived mode-specific ultimate strength formulae from a large nonlinear finite element dataset, but their design variable set is the primary panel between ordinary stiffeners and does not address a secondary, locally fitted detail such as a carling, nor the effect of that detail's weld connectivity on the panel's collapse mechanism. Sholikhah et al. [11] benchmarked the finite element buckling response of stiffened panels with flat-bar, angle, and Tee-bar stiffener sections, reporting substantially higher

compressive capacity for angle and Tee sections than flat bars; however, their comparison is made at a fixed, continuous, fully welded arrangement and does not vary the connectivity, offset, or continuity of the stiffener itself, which is the variable of interest in the present study. Hanif et al. [12] quantified how initial-imperfection mode, amplitude, slenderness, and span/bay ratio jointly affect ultimate strength and regressed a simplified formula, with 2.08 % error against FEM results, covering this parameter space; their formula is intended for panels without local secondary details, and does not consider a carling or similar local stiffening member, nor the adopted b/200 imperfection amplitude applied consistently across a parametric offset set as is done here. Li et al. [13] assessed the effect of welding-induced residual stress on the ultimate compressive strength of longitudinally stiffened panels through a parametric nonlinear finite element study, isolating residual stress as the single variable on an otherwise fixed, continuously welded panel; their work does not examine how removing a weld at a local detail, as in the present unwelded carling arrangement, changes the collapse mechanism, which is one reason residual stress is treated as a limitation of the present analysis (Section 2.7).

A second group of studies has focused on local connection details and damage rather than intact primary panels. Park and Yi [14] diagnosed in-service thin-plate buckling at a tanker aft-end panel reinforced with carlings and represented initial deflection by an eigenmode-based nodal offset; their work confirms the relevance of carling restraint but does not quantify nonlinear reserve. Bahmani et al. [15] showed that a stiffener discontinuity can change ultimate strength and failure mode, although their discontinuity resulted from damage rather than an intentional production detail. Silva-Campillo et al. [16] optimized a corner-bracket configuration by linear buckling analysis and testing, providing a close example of a local detail altered for practical benefit. The present study extends this line of work by determining whether the elastic-buckling change produced by carling removal also changes the Ultimate Strength under the same load pattern.

A third group addresses time-dependent degradation rather than a design-stage change in arrangement. Vu et al. [17] combined initial distortion, residual stress, and uniform corrosion in a single nonlinear finite element study of a bulk-carrier outer-bottom panel, quantifying strength loss over a 30-year service life; because this addresses degradation of a fixed structural arrangement, the interaction of corrosion with the carling offset comparison made here is identified as future work (Section 5). Saad-Eldeen and Garbatov [18] combined compressive collapse testing and nonlinear finite element analysis of corroded, perforated stiffened plates to derive regression equations for ultimate capacity as a function of opening degree; that study combined physical testing with nonlinear finite element analysis, whereas the present study is purely numerical, and it addresses a different discontinuity (an opening) rather than a local stiffener arrangement change, without comparison against a linear eigenvalue ranking.

Fhandy et al. [19] showed that the stiffening configuration of a ship stiffened panel markedly changes its crashworthiness under idealized penetration loading and that the numerical accuracy is strongly mesh-dependent, a 10 mm mesh reproducing the experimental benchmark within 5 %. Tu et al. [20] evaluated the structural strength of a planing hull by mapping the pressure field of a CFD analysis onto a structural finite element model in a one-way coupled procedure, which is analogous in principle to the global-to-local transfer of boundary deformation and pressure adopted here. Lee and Jung [21] demonstrated, using a single-degree-of-freedom model of hull plating, that the displacement response is governed mainly by the load impulse, whereas the strain-rate response is governed by the rate of load application; the structural relevance of a detail therefore depends on the characteristics of the governing load. Rognoni et al. [22] showed experimentally that local modifications integrated into a ship stiffened panel can suppress targeted low-frequency vibration modes, indicating that a change in local stiffening detail may alter dynamic behaviour even when static strength is unaffected. None of these studies, however, examines whether an empirically repeated secondary stiffener can be reduced without loss of nonlinear load-carrying capacity.

Finally, Jeong et al. [23] proposed a process-based modelling method describing ship block assembly planning that captures the organic relationships between fabrication, outfitting, and erection activities; this represents production-sequencing constraints and flexibility at the planning-system level but does not evaluate the structural consequence of a specific detail change. It is cited here to support the fabrication-sequencing motivation of Section 4.4, which the structural-mechanics literature reviewed above does not address.

The reviewed studies address panel collapse, local details, degradation and production planning, but do not quantify the present carling comparison under combined lateral pressure and transferred hull deformation. The contribution is the application and the observed difference in sensitivity: removal of two carlings reduces the elastic buckling factor by approximately 5.8 %, whereas the reported Ultimate Strength changes by approximately 0.5 %. The analysis methods themselves are established procedures, not a new numerical method.

1.4 Research gap, objectives, and contribution

This study quantifies how the number, offset and connection of local carlings influence elastic buckling and nonlinear resistance of one FLNG bulkhead. The physical finding concerns this geometry and load combination; it is not a universal rule for carling removal.

Five alternatives use the same reported boundary transfer and material formulation. Type 01 has three aligned carlings; Type 03 has one unwelded carling at 50 mm offset. This comparison includes both connection and number changes. Type 02 versus Type 03 isolates removal of the two upper carlings at the same offset. Types 03 to 05 examine offset sensitivity. A reduction from three parts to one is a count reduction, not a measured production saving.

The objectives are to distinguish elastic modal restraint from nonlinear resistance and to identify the limits of a fabrication motivated change. The sequence is adopted because an elastic eigenvalue alone does not quantify the response of an imperfect elastic plastic panel. Production benefits are conditional on further load, fatigue and shop verification.

2. Materials and methods

2.1 Structural configuration and design alternatives

The investigated region is a transverse bulkhead panel at a mid-hold frame of a floating liquefied natural gas (FLNG) unit. The plating is supported by regularly spaced ordinary vertical stiffeners and by locally fitted horizontal carlings. The five alternatives shown in Fig. 1 were selected to separate two structural variables: (i) continuity and population of the carling system and (ii) the offset of the remaining carling from the ordinary stiffener. This distinction is essential because the former changes the effective rotational restraint and elastic buckling mode, whereas the latter mainly changes the local position at which stiffness is introduced into the plate-stiffener assembly.

Type 01: three carlings are fitted within the examined height, and each carling web is aligned with, and directly welded to, the ordinary stiffener at the intersection, providing a continuous, welded load path between the carling and the stiffener.

Type 02: the three-carling system is retained, but the lowest carling is offset by 50 mm from the ordinary stiffener centreline and the intersection is not welded (“NO WELDING”), so that the carling and the stiffener are not directly connected at that location.

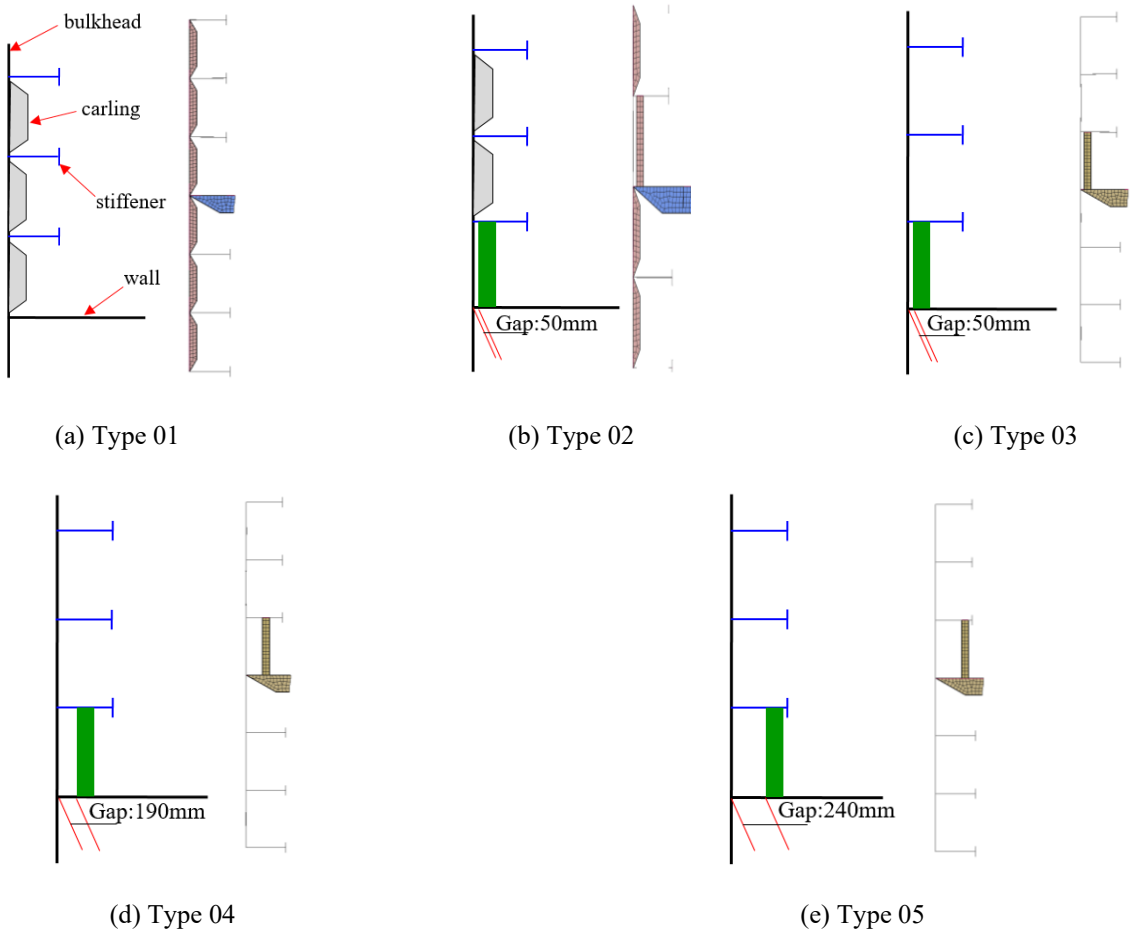
Types 03-05: the two upper carlings are removed, and a single unwelded carling is retained at an offset of 50 mm, 190 mm, and 240 mm from the ordinary stiffener centreline, respectively.

All five arrangements were evaluated for the same panel geometry, plating thickness, stiffener scantlings, and loading; the finite element models differ only in the carling population, position, and connectivity described above. Mesh density, material properties, boundary conditions, and the applied load case were kept identical for all models so that the comparison isolates the effect of carling arrangement.

Consequently, Type 01 versus Type 02 evaluates the local connection change while maintaining the carling population; Type 02 versus Type 03 evaluates the effect of removing the two adjacent carlings at the same 50 mm offset; and Types 03-05 evaluate offset sensitivity within an otherwise identical reduced-carling configuration. The five arrangements are summarised in Table 1 and shown in Figure 1.

Table 1 Summary of the five carling arrangements (Types 01-05)

Arrangement	Number of carlings	Offset of the lowest (or single) carling from the stiffener centerline	Weld condition at intersection
Type 01	3	0 mm (aligned)	Welded
Type 02	3	50 mm	Not welded
Type 03	1	50 mm	Not welded
Type 04	1	190 mm	Not welded
Type 05	1	240 mm	Not welded



(a) Type 01 (b) Type 02 (c) Type 03

(d) Type 04 (e) Type 05

Fig. 1 Carling configurations used in the finite element comparison: Types 01-02 retain three carlings, whereas Types 03-05 retain one unwelded carling at increasing offset

Figure 1 defines the five model configurations and the variables used in the comparative assessment. Type 01 provides the greatest local continuity because all three carlings intersect the ordinary stiffener without an intentional gap. Type 02 retains the same three-member system but introduces a 50 mm offset and an unwelded intersection at the lowest carling. Type 03 has the same 50 mm offset as Type 02 but omits the two upper carlings, thereby reducing the distributed transverse restraint over the panel height. Types 04 and 05 maintain this single-carling topology while increasing the offset to 190 and 240 mm. The model series is therefore not a pure one-parameter offset study: the marked change between Types 02 and 03 includes a change in carling population, while the comparison among Types 03-05 isolates the influence of offset. This distinction is used in interpreting the eigenvalue and nonlinear results.

2.2 Material properties and constitutive model

The model contains mild steel with nominal engineering yield stress 235 MPa and HT32 steel with nominal engineering yield stress 315 MPa. HT32 is retained as the project grade designation; “S315” in the supplied input denotes the project material curve and is not asserted to be a directly tabulated DNV steel grade.

The common elastic reference is E = 210,000 MPa, Poisson ratio 0.30 and density 7,850 kg/m³ (7.85×10^{-6} kg/mm³). Nominal yield stresses and true stress curve ordinates are different measures and are not interchangeable.

Table 2 Linear elastic material properties

Material	Elastic modulus, E [MPa]	Density, ρ [kg/mm³]	Poisson's ratio, ν	Specified minimum yield stress, σ_Y [MPa]
MILD (S235)	210,000	7.85×10^{-6}	0.3	235.0
HT32 (S315)	210,000	7.85×10^{-6}	0.3	315.0

The constitutive description follows the idealized steel material approach in DNV RP C208 [24]. Table 3 retains the supplied project curve parameters rather than replacing them by a different steel grade. The 235 MPa nominal yield stress corresponds to a true stress ordinate of 236.2 MPa in the supplied mild steel curve; the corresponding HT32 ordinates are 315 and 317 MPa. True stress accounts for the current area, while logarithmic strain accumulates finite deformation. Before necking in uniform uniaxial tension, $\sigma_{true} = \sigma_{eng}(1 + \varepsilon_{eng})$, $\varepsilon_{ln} = \ln(1 + \varepsilon_{eng})$, and $\varepsilon_p = \varepsilon_{ln} - \sigma_{true}/E$. The solver input must distinguish total from plastic strain. Cauchy stress must be used with the solver's consistent finite strain formulation; Cauchy stress and logarithmic strain are not an unrestricted work conjugate pair for arbitrary multiaxial deformation. E = 206,000 MPa in the earlier elastic table has been removed from the harmonized reporting basis. No new solver analyses were performed for this editorial revision, so agreement of the archived elastic material cards with the harmonized value remains a verification limit, rather than an assumed numerical result.

Table 3 DNV RP C208 [24] based project curve parameters for t ≤ 16 mm

Parameter	S235	S315
Elastic modulus, E [MPa]	210,000	210,000
Proportional limit, σ_{prop} [MPa]	211.7	284.0
Yield stress, σ_{yield} [MPa]	236.2	317.0
Secondary yield stress, σ_{yield2} [MPa]	243.4	325.0
Plastic strain at yield, $\varepsilon_{p,y1}$	0.004	0.004
Plastic strain at secondary yield, $\varepsilon_{p,y2}$	0.0198	0.016
Strength coefficient, K [MPa]	520.0	683.0
Strain-hardening exponent, n	0.166	0.166

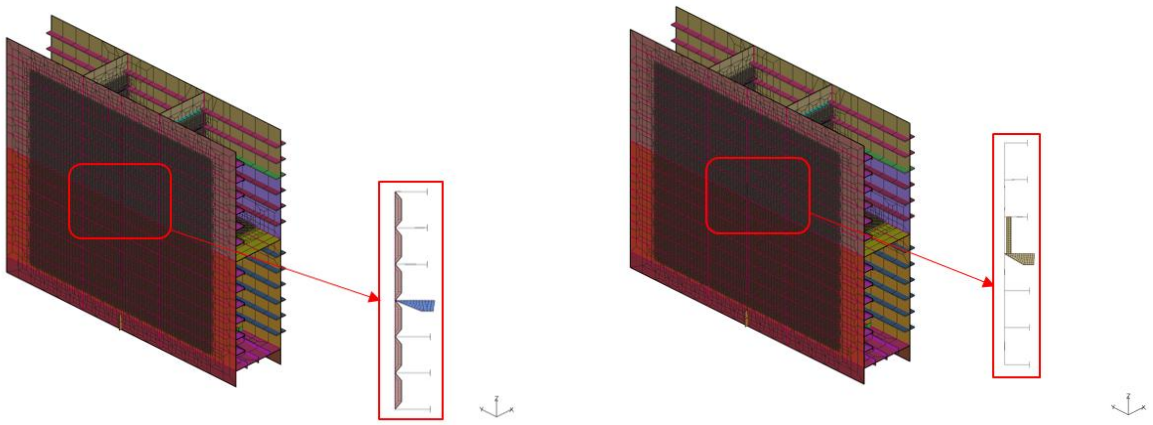
2.3 Finite element modelling and sub-modelling strategy

A global-to-local sub-modelling approach was adopted. A full-hull (global) finite element model was first analysed under the governing design load case, and the resulting displacement field at the boundary of the region of interest was extracted and imposed as enforced displacements (SPCD) on the boundary of a fine-mesh local sub-model, together with the corresponding local pressure loads. This approach allows the local carling detail to be represented with a mesh fine enough for buckling and nonlinear collapse analysis while retaining the overall stiffness and load path context of the global hull structure. A comparable one-way transfer of loads from a global analysis to a structural finite element model has recently been used to evaluate the structural strength of a planning hull [20].

The sub-model for all five arrangements covered the same spatial domain, defined in the global model coordinate system by $X = 115{,}600–118{,}600$ mm, $Y = 7{,}515–22{,}905$ mm, and $Z = 12{,}515–25{,}340$ mm, and used two-dimensional shell elements with an average mesh size of 50 mm × 50 mm in the fine-mesh area surrounding the carling detail. The resulting mesh statistics are summarised in Table 4; the models differ only marginally in node and element count as a direct consequence of the local carling geometry change.

Table 4 Sub-model mesh statistics

Model	Element type	Average mesh size	Nodes	Elements
Type 01	2D shell	50 mm × 50 mm	145,095	146,833
Type 02			144,773	146,474
Type 03			144,773	146,474
Type 04			144,773	146,474
Type 05			144,773	146,474



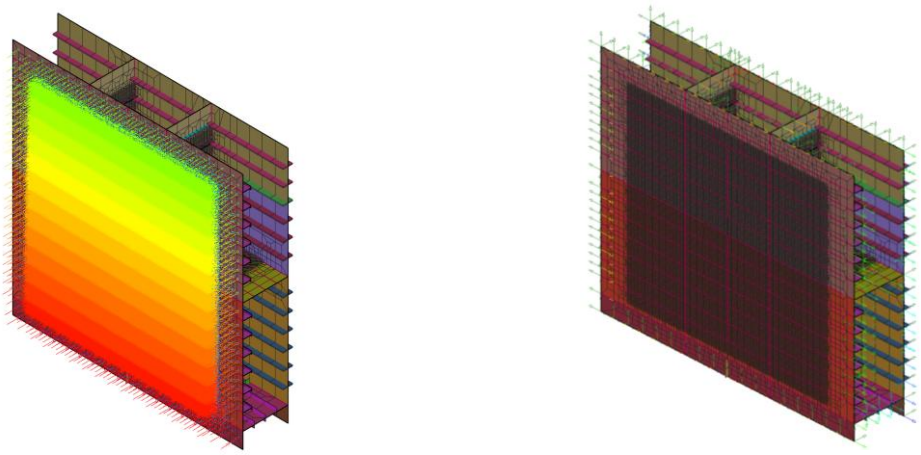
(a) type-01 model (b) type-03 model

Fig. 2 Global-to-local finite element models for (a) Type 01 and (b) Type 03; the inset identifies the fine-mesh carling region

Figure 2 shows the local shell models for the most highly restrained configuration (Type 01) and the reduced-carling configuration (Type 03). The same cut-boundary location, panel extent, ordinary stiffeners, and fine-mesh region are retained in both models; only the carling arrangement is changed. The local mesh resolves the plate bays and the web-flange junctions that participate in the observed multi-half-wave buckling mode. Because the transferred displacement boundary is located away from the carling intersection, the comparison is not dominated by an artificial constraint at the detail. The close global-local agreement subsequently demonstrated in Figure 9 confirms that this cut-boundary selection transmits the global hull deformation without introducing a spurious local stiffness discontinuity.

2.4 Loading and boundary conditions

The Design Load combines enforced nodal boundary displacements transferred from the global full hull analysis with local depth dependent hydrostatic pressure. The same reference loading pattern is used for all arrangements. In the nonlinear comparison, λ denotes the multiplier of this reference state; the design point is $\lambda = 1$.



(a) hydro static pressure

(b) constraint displacement induced by global and local loads

Fig. 3 Combined sub-model loading: (a) depth-dependent hydrostatic pressure and (b) enforced boundary displacements transferred from the global model

Figure 3 illustrates the two complementary components of the sub-model loading. The depth-dependent pressure in Figure 3a produces local plate bending and stiffener reactions, while the enforced displacement field in Figure 3b introduces the hull-girder and surrounding-structure deformation obtained from the global analysis. Applying pressure alone would omit the membrane and frame-deformation components of the actual load path; applying transferred displacements alone would omit the local lateral-pressure demand. Their simultaneous application therefore reproduces the combined stress state required for a meaningful stability assessment. Identical pressure and boundary-displacement fields were used for every carling arrangement, so differences in response can be attributed to model topology rather than to loading inconsistency.

2.5 Buckling and nonlinear analysis procedure

Each sub-model was subjected to three sequential analyses. First, a linear static solution established the reference stress field under DL. Second, the linear buckling eigenvalue problem was solved:

$$(\boldsymbol{K} + \lambda \boldsymbol{K}_{\mathrm{G}})\boldsymbol{\varphi} = 0 \tag{1}$$

where $\boldsymbol{K}$ and $\boldsymbol{K}_G$ are elastic and geometric stiffness matrices, λ is the Design Load multiplier, and φ is the buckling eigenvector. The first eigenvalue $\lambda 1$ characterizes elastic instability of the ideal model. The imperfect nonlinear model supplies the load displacement path. A denotes λ = 1, or 100 % Design Load; B denotes Ultimate Strength, λ_u, by the intersection of the elastic and plastic branch lines. These two tangent estimates differ from a directly observed curve peak and from first yield.

$$\lambda_e(u) = k_e u + c_e$$
$$\lambda_p(u) = k_p u + c_p \tag{2}$$

$$u_B = (c_p - c_e)/(k_e - k_p)$$
$$\lambda_u = k_e u_B + c_e \tag{3}$$

$$Design\ Load\ percentage = 100\lambda$$
$$A: \lambda = 1 \tag{4}$$
$$B: \lambda = \lambda_u$$

The slopes k_e and k_p and intercepts c_e and c_p describe representative branches before and after pronounced stiffness reduction, excluding the transition. B is their intersection and may lie off the curved response. Redrawn graphs use the supplied raster curves, reported strength ordinates and approximate B displacements. They illustrate the criterion without independently reproducing unavailable solver histories or quantifying fitting uncertainty.

2.6 Assessment sequence

Figure 4 links the common loading, constitutive model, geometric imperfection and mesh verification to the arrangement comparison. Model resolution is selected for the response quantities being compared, rather than from an elastic displacement check alone. Linear response, elastic buckling and nonlinear load redistribution are then evaluated on the adopted 50 mm mesh. *A* is 100 % Design Load; *B* is Ultimate Strength by the elastic and plastic branch intersection. The final decision distinguishes a permissible design opportunity under the studied loading from verification required for other limit states.

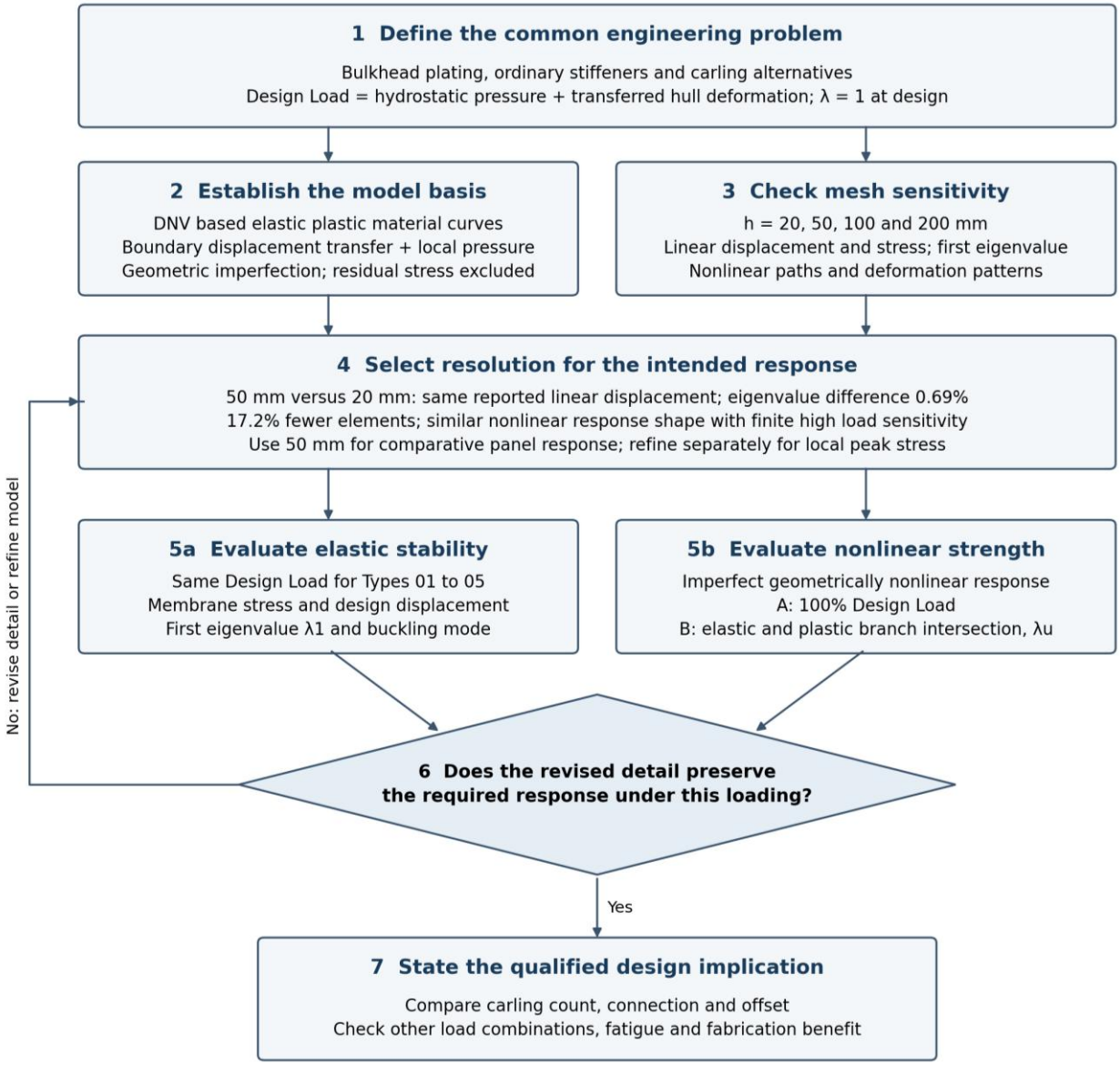
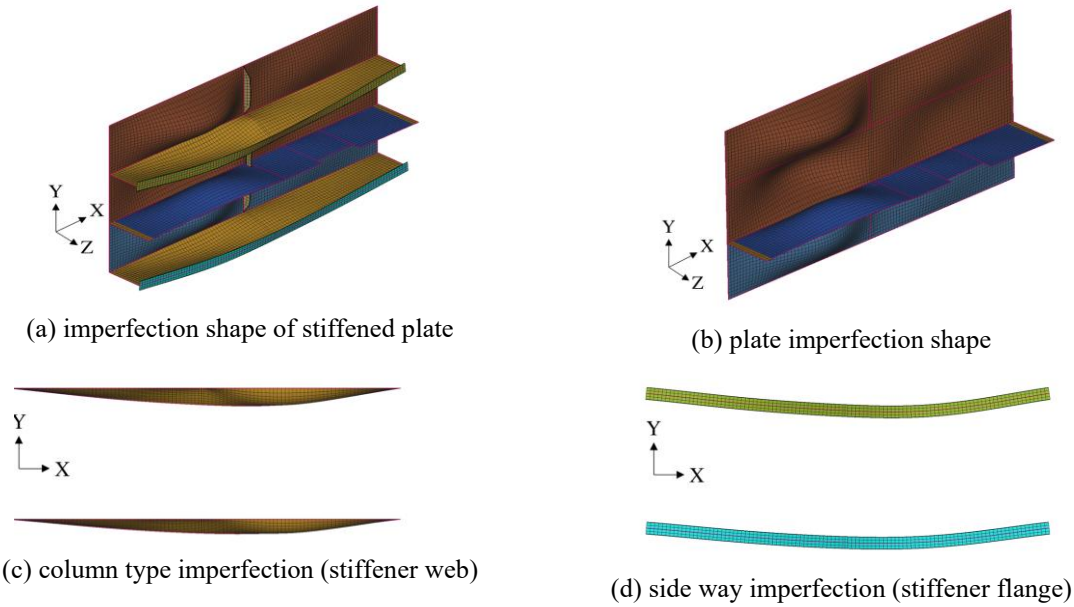


Fig. 4 Complete assessment methodology including mesh selection, parallel elastic and nonlinear checks, and the decision to retain or revise a carling arrangement

2.7 Initial geometric imperfection

The original arrangement comparison uses an eigenmode shaped initial imperfection with maximum amplitude b/200. The additional mesh study explicitly reports b/200 = 4.275 mm, corresponding to b = 855 mm, and labels its imperfection shape as buckling mode 2. It therefore cannot be described as an identical first mode study without checking the input decks. The amplitude is treated here as an adopted modelling assumption; an exact IACS provision prescribing this value has not been established in the supplied evidence. The nonlinear response includes geometric imperfection, but excludes welding residual stress. Sensitivity to mode, amplitude and residual stress has not been demonstrated.



(a) imperfection shape of stiffened plate

(b) plate imperfection shape

(c) column type imperfection (stiffener web)

(d) side way imperfection (stiffener flange)

Fig. 5 Type 01 eigenmode-affine initial imperfection: (a) complete stiffened panel, (b) plate, (c) stiffener web, and (d) stiffener flange

Figure 5 separates the imposed imperfection into the plate, stiffener-web, and stiffener-flange components of the Type 01 model. The displayed deformation is magnified 100 times for clarity; the numerical amplitude used in the nonlinear model is $b/200$. The plate component contains the dominant multi-half-wave out-of-plane pattern, while the web and flange components preserve compatibility at the plate-stiffener junction. Using the complete eigenvector rather than imposing an independent sinusoidal plate imperfection avoids an artificial mismatch between connected shell components. It also introduces the most readily excited instability pattern into the nonlinear solution, thereby reducing the unrealistically high resistance that can be obtained from a perfectly flat, perfectly symmetric model. The selected amplitude represents a fabrication-level geometric imperfection; welding residual stress is not included and remains a limitation of the computed capacity.

2.8 Mesh sensitivity and engineering selection of the 50 mm mesh

A reference submodel was examined using local shell sizes of 20, 50, 100 and 200 mm over the same spatial domain. They are denoted M20, M50, M100 and M200 to distinguish mesh cases from the five carling arrangements. Mesh validity is assessed against three response classes: linear stiffness and local stress resolution, elastic instability, and nonlinear response including the deformation pattern. The finest mesh is a numerical reference rather than an exact solution. The objective is to select a suitable discretization for the comparative panel study, not to establish mesh independent weld toe or fatigue stresses.

Table 5 Mesh sensitivity under DL

Case	h mm	Nodes	Elements	Peak stress MPa	Max u mm	First eigenvalue
M20	20	175006	177354	378.6	101.9	1.410
M50	50	145095	146833	309.0	101.9	1.400
M100	100	138004	139586	267.2	101.9	1.397
M200	200	136929	138424	205.0	101.7	1.396

Linear response and elastic instability. Table 5 reports mesh size, model size and the analysis outputs. Relative differences are evaluated as $\delta q = 100|q(h) - q(20)|/|q(20)|$. Maximum linear displacement is 101.9 mm for the 20, 50 and 100 mm models and 101.7 mm for 200 mm. Thus 50 mm preserves the reported displacement at the available 0.1 mm precision. The first eigenvalue is 1.400472 at 50 mm compared with 1.410221 at 20 mm, a difference of 0.691 %. The 100 and 200 mm differences are 0.902 % and 0.944 %,

respectively. Figure 6 distinguishes stable overall response from the continuing sensitivity of the local stress maximum.

The peak linear von Mises stress rises from 205.0 MPa at 200 mm to 267.2, 309.0 and 378.6 MPa at 100, 50 and 20 mm. At 50 mm it remains 18.38 % below the finest mesh peak. Consequently, agreement in displacement or eigenvalue cannot establish convergence of stress near a geometric discontinuity. These localized peaks are also distinct from the component membrane stresses used in the arrangement comparison. The 50 mm choice is justified for overall panel response; it is not a resolved local peak stress assessment.

Resolution and model size. The 50 mm model contains 146,833 shell elements instead of 177,354 at 20 mm, a reduction of 17.21 %, and 145,095 rather than 175,006 nodes, a reduction of 17.09 %. Moving from 100 to 50 mm adds only 5.19 % to the whole submodel element count while doubling local linear resolution. With the reported plate breadth of 855 mm, the nominal number of elements across the breadth increases from about 8.6 at 100 mm to 17.1 at 50 mm, compared with 42.8 at 20 mm. These values explain the practical benefit of resolving the local plate and stiffener fields without using the finest tested discretization everywhere. Element count indicates model size; no measured CPU time reduction is inferred.

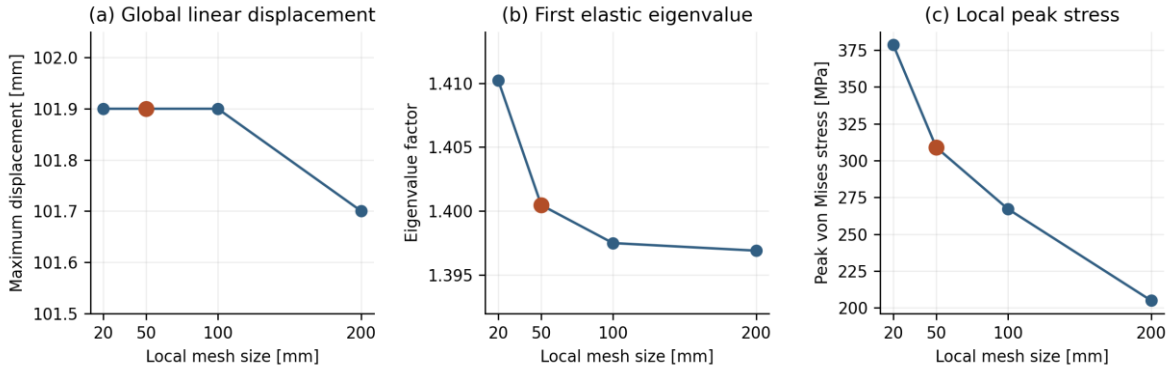


Fig. 6 Mesh sensitivity of global displacement, first eigenvalue and local peak stress. The highlighted 50 mm point preserves overall stiffness and elastic instability closely while local peak stress remains sensitive

Nonlinear response. The overlaid curves in the supplied presentation follow a similar initial path and develop a common transition toward lower tangent stiffness. Figure 7 retains the individual elastic and plastic branch constructions, with A at 100 % Design Load and B at the two tangent Ultimate Strength. The mesh runs report B at approximately 200 %, while the arrangement series reports 219 to 221 %; these are retained as separate datasets. The panels use the rounded source B ordinates for normalization, so their identical 200 % labels are not an independent convergence measurement.

Table 6 is a graphical sampling of the supplied curves, not an export of solver data. Here $\eta = q/q_{ref}$, where q is the original common plotted load ordinate and q_{ref} is its final common value of 100; η is used only for cross mesh response comparison and is not an additional definition of Design Load. At $\eta = 0.40$, the 50 mm displacement differs from the 20 mm estimate by approximately 0.7 %. The difference increases to about 2.7 % at $\eta = 0.80$ and 6.4 % at the final common ordinate. Thus, response similarity is strongest before and around stiffness reduction and is finite at higher loading. At the latter levels, the 50 mm model is slightly more compliant than the 20 mm model, rather than being artificially stiffer. These approximate values characterize path sensitivity and do not establish convergence of the fitted Ultimate Strength factor.

Table 6 Approximate displacement at common ordinate levels of the source nonlinear plots

Mesh h [mm]	u at $\eta = 0.40$[mm]	u at $\eta = 0.80$[mm]	u at $\eta = 1.00$[mm]	Δu at $\eta = 1.00$ versus M20 [%]
20	≈45.5	≈99.3	≈147.0	≈+0.0
50	≈45.8	≈102.1	≈156.4	≈+6.4
100	≈46.0	≈99.4	≈150.5	≈+2.4
200	≈43.9	≈98.8	≈150.5	≈+2.4

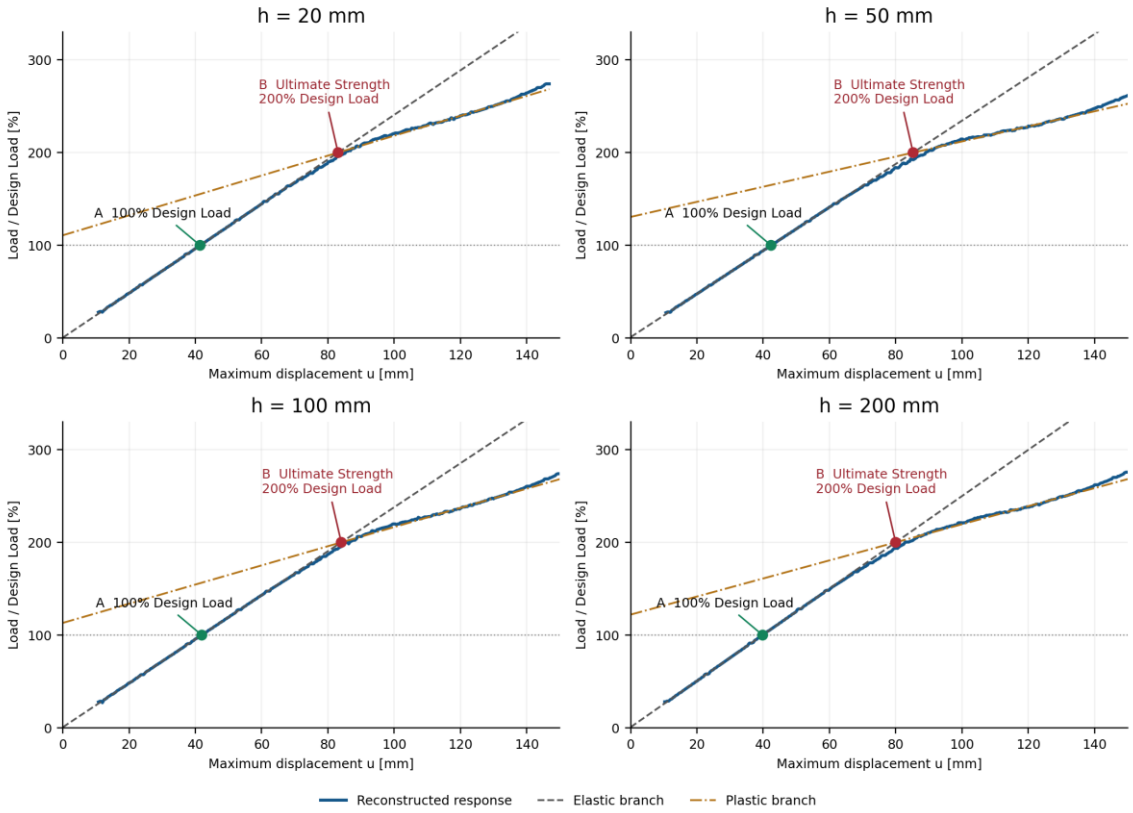


Fig. 7 Nonlinear mesh responses with A at 100 % Design Load and B at Ultimate Strength by elastic and plastic branch intersection. Curves are reconstructed from the supplied graphics; rounded B values provide normalization, while Table 6 samples cross mesh displacement independently of these labels

The nonlinear fields in Figure 8 show distributed plate and stiffener response rather than a new isolated deformation mechanism appearing only at 50 mm. The coarsest discretization renders the local gradients more crudely, while the two finer meshes resolve similar broad deformation regions. This qualitative agreement supports the use of the 50 mm discretization to compare arrangements, but neither contour similarity nor the rounded B annotations proves that the local stress maximum or the Ultimate Strength fitting error is negligible.

Engineering selection. The combined evidence supports 50 mm as a practical resolution for the present comparative panel analysis: design displacement is unchanged at the reported precision, elastic instability differs by less than 0.7 % from the 20 mm reference, and the nonlinear paths and broad deformation patterns remain consistent while high load compliance retains finite sensitivity. The choice also provides approximately 17 elements across the reported plate breadth at a lower total model size than the 20 mm case. The data do not establish a unique mathematical optimum, because cost versus error weights and measured solver times are unavailable. In this engineering sense, 50 mm is an effective balance of response fidelity, local resolution and model size; peak stress, weld detail, imperfection mode sensitivity and the reduced carling case require their own verification when those quantities govern.

The supplementary mesh model reports a mode 2 imperfection of 4.275 mm, whereas the arrangement description uses the first mode. In addition, the supplementary 100 mm eigenvalue of 1.397497 is close to the original arrangement reference of approximately 1.397. The two datasets are therefore not silently substituted. The mesh study establishes a documented engineering basis for selecting resolution; it does not remove these model record and comparability limits.

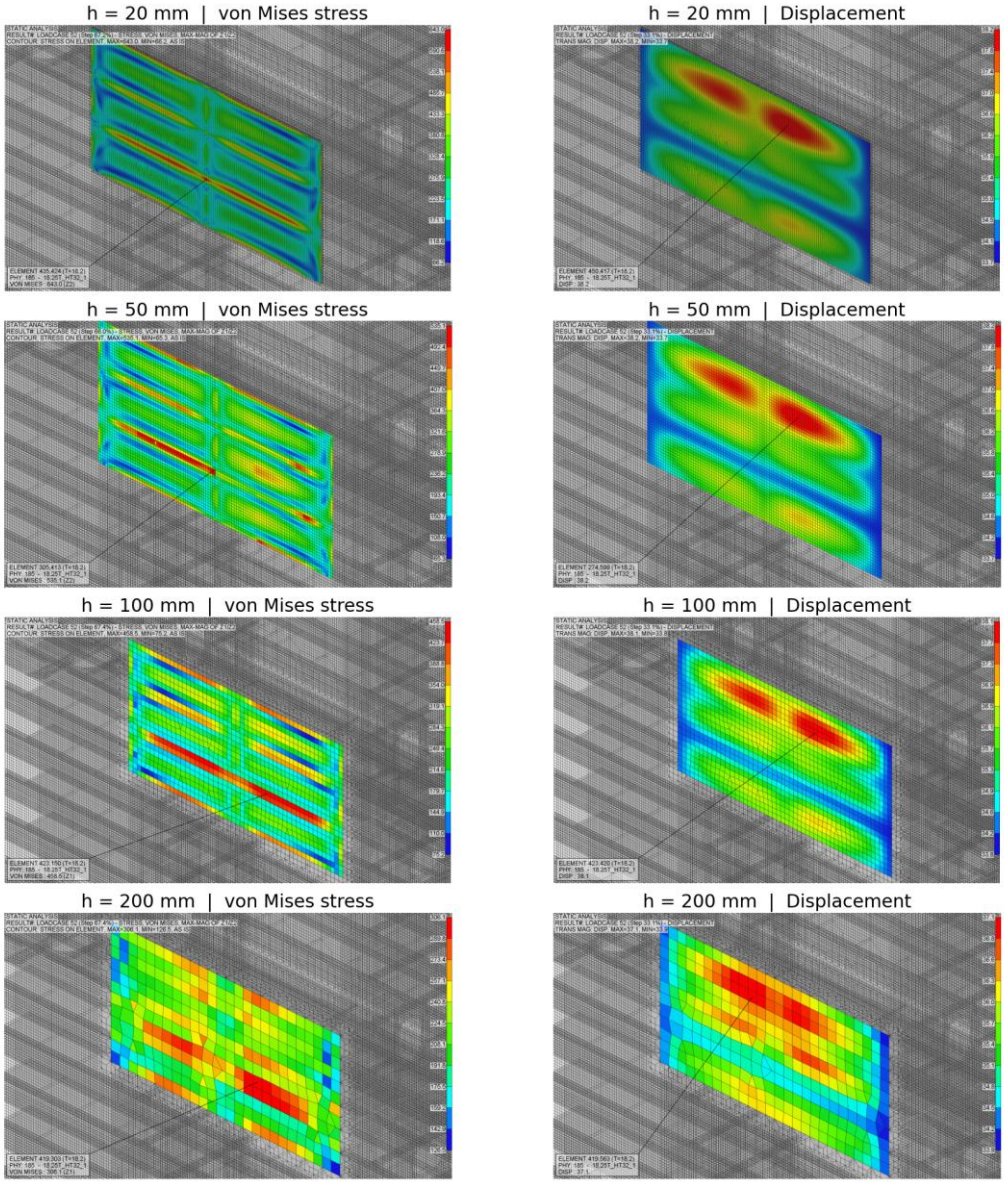


Fig. 8 Nonlinear stress and displacement fields for the four local mesh sizes at the reported B state of the mesh study. Contours are retained from the supplied analysis. Individual legends are retained, so comparison concerns field distribution rather than equal colors across different scales

3. Results

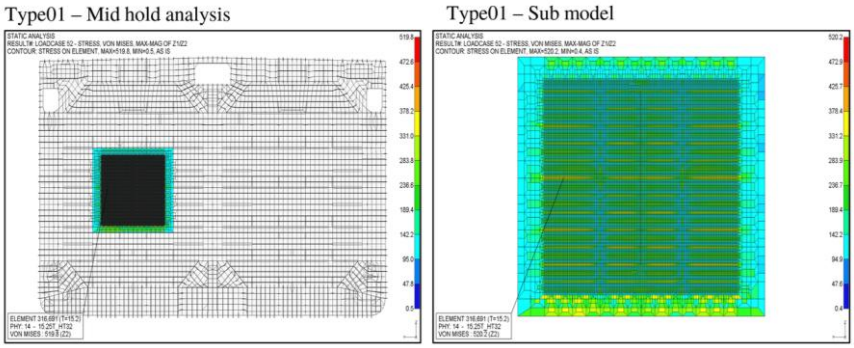
3.1 Global-to-local verification

Figure 9 provides a consistency check of the displayed global and local fields under DL: the reported peak stresses differ by less than 0.1 %, and the maximum displacement is 102.3 mm. This agreement is useful but does not establish force equilibrium, adequacy of boundary distance or convergence of local stress and nonlinear resistance. The archived data do not specify the complete transferred degree of freedom set, interpolation algorithm or reaction balance. These limitations are distinct from the mesh study in Section 2.8.

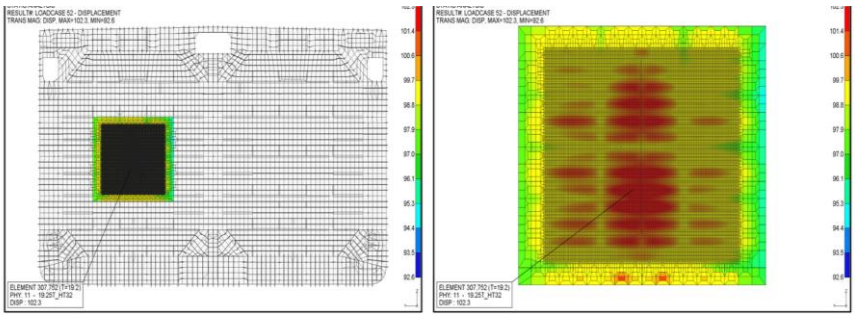
3.2 Linear elastic stress and displacement response

Under the design load case (DL), the linear elastic stress and displacement responses of all five carling arrangements were similar in magnitude, as summarized in Table 7. The maximum von Mises stress in the plate was 194.9 MPa for Type 01 and Type 02, and 191.5 MPa for Type 03-05; the maximum von Mises stress at the stiffener was 300.7 MPa for Type 01, 301.0 MPa for Type 02, and 298.7 MPa for Type 03-05; and the maximum displacement in way of the carling was 102.3 mm for Type 01 and Type 02, and 102.6 mm for Type

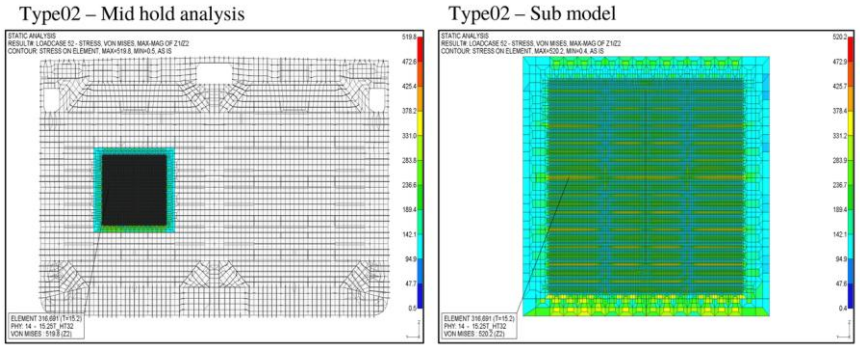
03-05. The five arrangements are therefore essentially equivalent from a linear elastic design-check standpoint, with differences of the order of 1.7 % or less in every reported quantity.



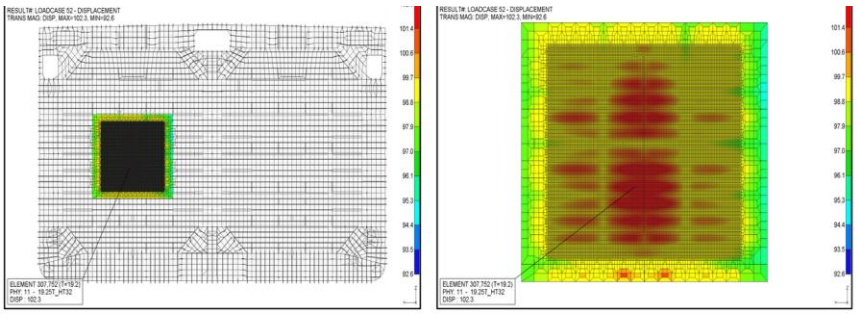
(a) Type 01 (von Mises stress)



(b) Type 01 (displacement)



(c) Type 02 (von Mises stress)



(d) Type 02 (displacement)

Fig. 9 Global-to-local verification under DL: von Mises stress and displacement for (a,b) Type 01 and (c,d) Type 02

Table 7 Linear elastic FE results under the design load case (DL)

Quantity	Location	Type 01	Type 02	Type 03	Type 04	Type 05
Von Mises stress, membrane [MPa]	Plate	194.9	194.9	191.5	191.5	191.5
	Stiffener	300.7	301.0	298.7	298.7	298.7
Displacement [mm]	All	102.3	102.3	102.6	102.6	102.6

The reported membrane stresses are approximately 81 to 83 % of nominal plate yield and 95 to 96 % of nominal stiffener yield. These linear response quantities differ little between arrangements, suggesting that the ordinary stiffeners and plating dominate the design load response. Such linear elastic ratios are not a nonlinear yielding or class acceptance check. Local mesh study peaks in Table 5 use a different stress extraction and must not be substituted for these component membrane values.

3.3 Linear eigenvalue buckling

The first eigenvalue factors, $\lambda 1$, read from Figure 10 are approximately 1.397, 1.399, 1.316, 1.317, and 1.316 for Types 01-05, respectively. Types 01 and 02 are effectively indistinguishable, indicating that offsetting and disconnecting only the lowest carling does not materially change the global elastic bifurcation threshold while the two upper carlings remain. The reduction occurs between Types 02 and 03, where the two upper carlings are removed; the first eigenvalue decreases by approximately 5.8 %. Types 03-05 then remain within about 0.1 % of one another, showing that the offset of the single remaining carling has little influence over the range considered. The eigenmodes remain plate-dominated, but the location and relative amplitude of the lobes change with the restraint pattern.

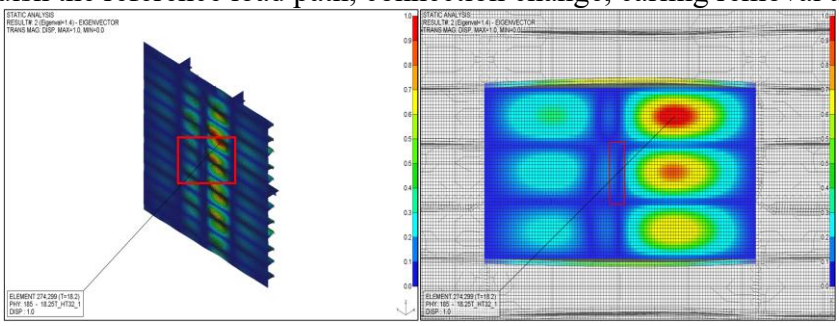
Figure 10 presents the normalized first eigenmode for each arrangement; the contours indicate relative modal displacement and do not represent the physical deformation at a specified load. Types 01 and 02 exhibit closely related multi-half-wave patterns because their distributed carling support is similar, consistent with their nearly equal eigenvalues. After the two upper carlings are removed in Type 03, the modal deformation becomes more continuous over the panel height and the eigenvalue falls to approximately 1.316. Types 04 and 05 show only minor redistribution of the dominant lobe as the single carling is shifted, which is consistent with the near-constant eigenvalue of the three reduced-carling models. The red box identifies the local carling position and demonstrates that the carling modifies the modal restraint locally rather than changing the instability into a stiffener-tripping or overall-column mode. The corresponding mode of each model was used as the initial-imperfection pattern in the nonlinear analysis, establishing the formal link between Figure 10 and Figures 12-16.

Figure 11 separates carling count from offset. Types 01 and 02 have similar elastic factors because the two upper carlings remain. Their removal in Type 03 lowers the factor, while further offset changes in Types 04 and 05 have little additional effect. The elastic trend therefore reflects the distributed modal restraint rather than the retained carling offset alone.

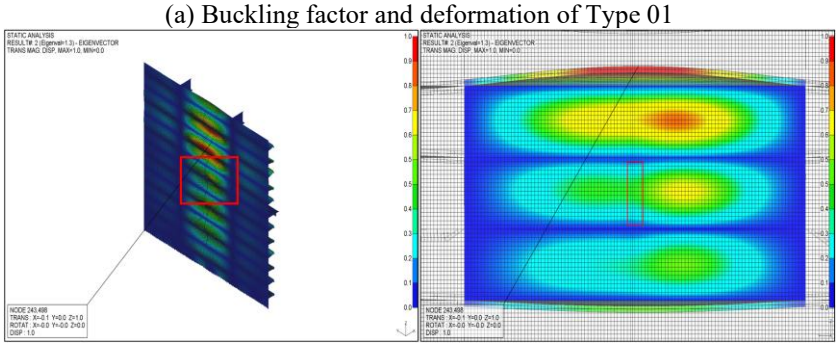
3.4 Nonlinear ultimate strength behaviour

Figures 12 to 16 apply the definitions in Section 2.5: A is 100 % Design Load and B is Ultimate Strength by the elastic and plastic branch intersection. Table 9 summarizes the common states. The figure

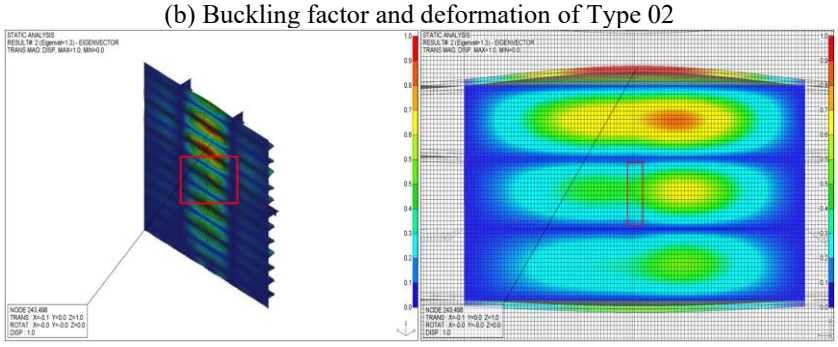
discussions distinguish the reference load path, connection change, carling removal and offset response.



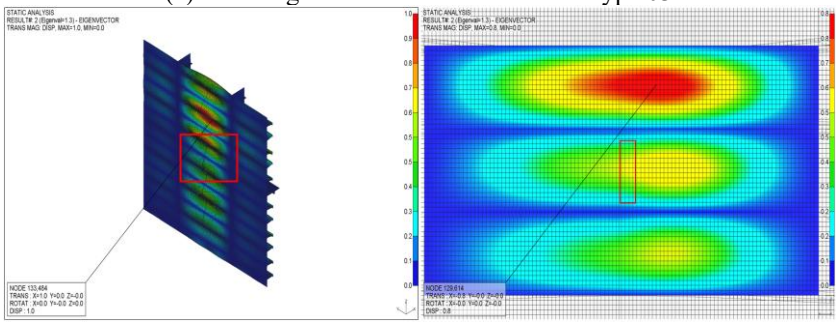
(a) Buckling factor and deformation of Type 01



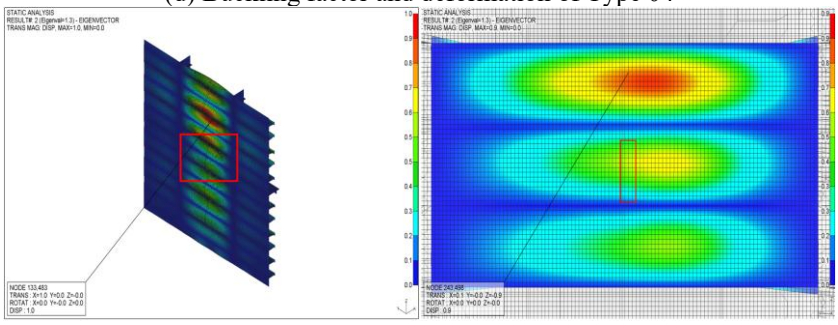
(b) Buckling factor and deformation of Type 02



(c) Buckling factor and deformation of Type 03



(d) Buckling factor and deformation of Type 04



(e) Buckling factor and deformation of Type 05

Fig. 10 First eigenvalue buckling modes for (a) Type 01, (b) Type 02, (c) Type 03, (d) Type 04, and (e) Type 05; red boxes indicate carling locations

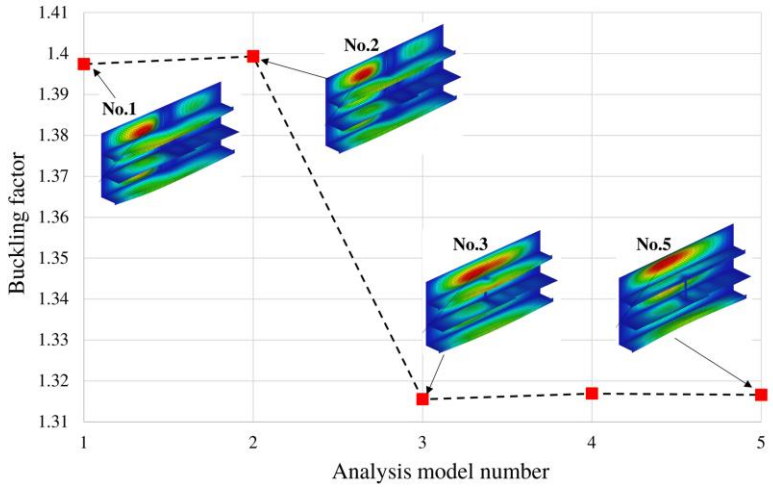
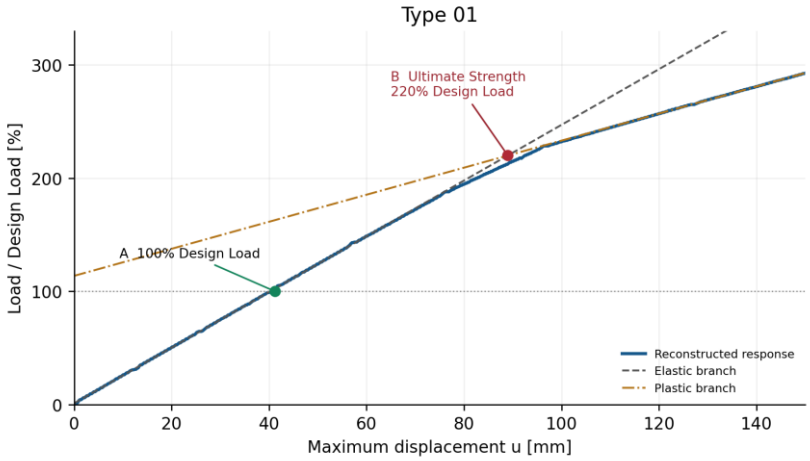
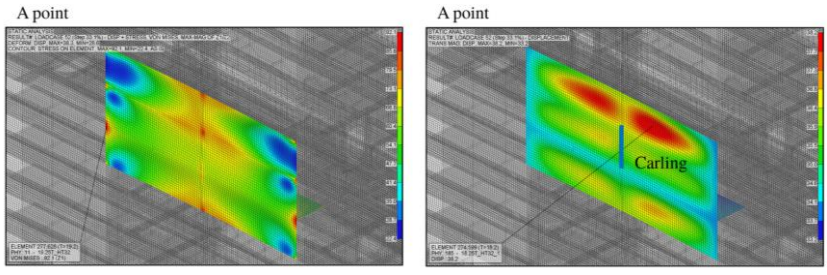


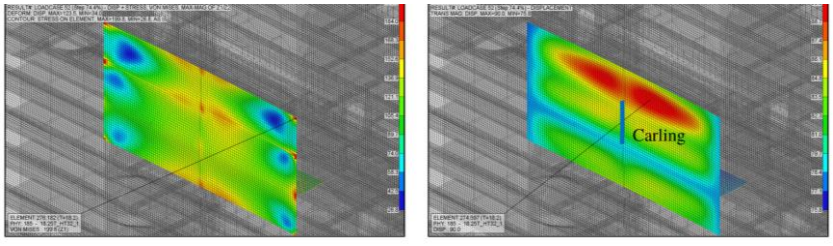
Fig. 11 First eigenvalue buckling factor for the five carling configurations



(a) Load displacement response with A at 100 % Design Load and B at Ultimate Strength

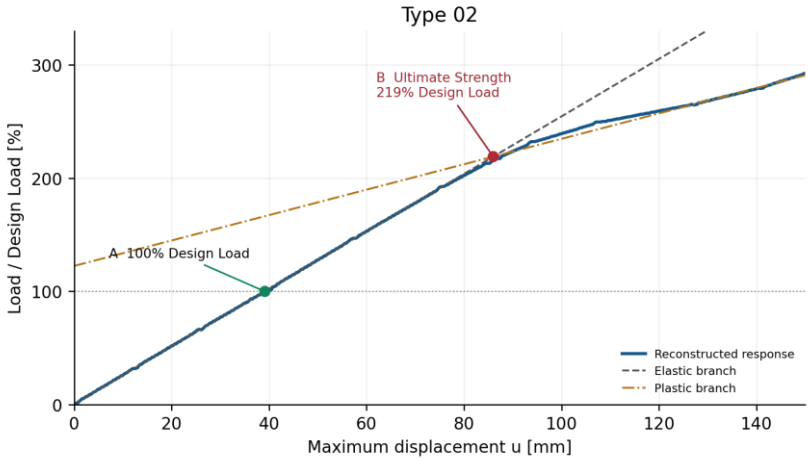


(b) Stress and displacement contours at A, 100 % Design Load

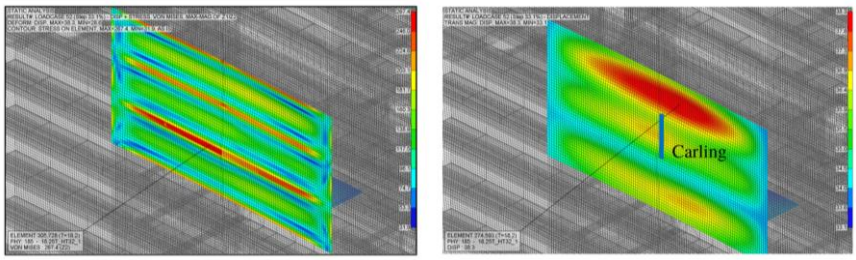


(c) Stress and displacement contours at B, Ultimate Strength

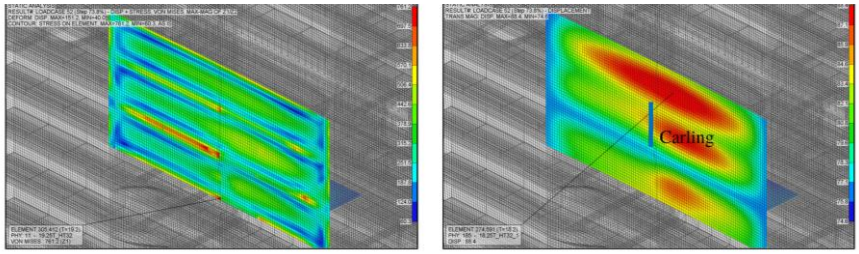
Fig. 12 Type 01 nonlinear response. A is 100 % Design Load and B is Ultimate Strength by the elastic and plastic branch intersection. The curve is a graphical reconstruction; the associated contours are retained from the supplied analysis



(a) Load displacement response with A at 100 % Design Load and B at Ultimate Strength



(b) Stress and displacement contours at A, 100 % Design Load



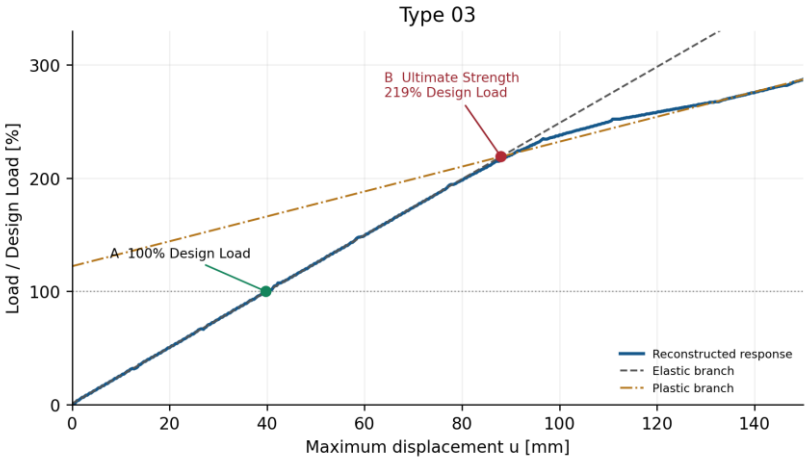
(c) Stress and displacement contours at B, Ultimate Strength

Fig. 13 Type 02 nonlinear response. A is 100 % Design Load and B is Ultimate Strength by the elastic and plastic branch intersection. The curve is a graphical reconstruction; the associated contours are retained from the supplied analysis

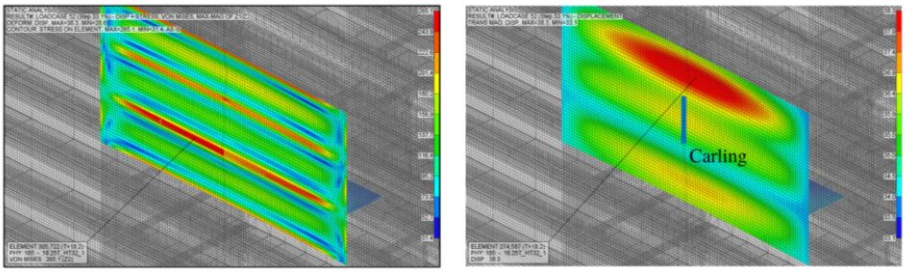
For the welded reference configuration, the distributed fields support panel wide load redistribution; the two tangent Ultimate Strength factor is 2.20.

Type 02 isolates the combined offset and connection change at the lowest carling while retaining the two upper members. Its $\lambda_u = 2.19$ differs little from the reference value, and the contour pattern does not reveal a new localized response at the unwelded intersection. The principal observation is therefore limited sensitivity to this particular connection change, rather than proof that weld continuity is irrelevant under every load combination.

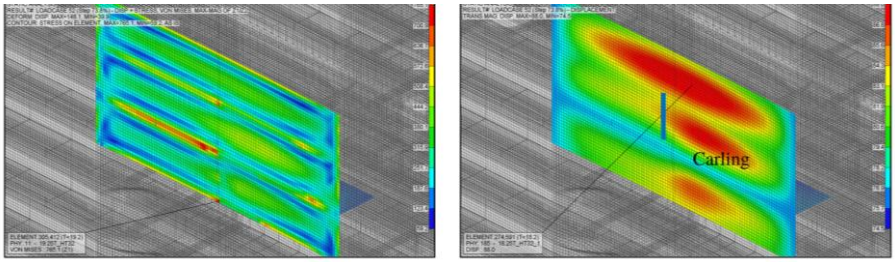
Type 03 removes the two upper carlings from the Type 02 configuration. This is the decisive comparison for carling count: elastic buckling resistance falls, while λ_u remains 2.19. The stress and displacement fields extend over the plate and ordinary stiffeners rather than concentrating exclusively at the retained carling. The result distinguishes loss of elastic modal restraint from loss of the nonlinear load redistribution mechanism.



(a) Load displacement response with A at 100 % Design Load and B at Ultimate Strength

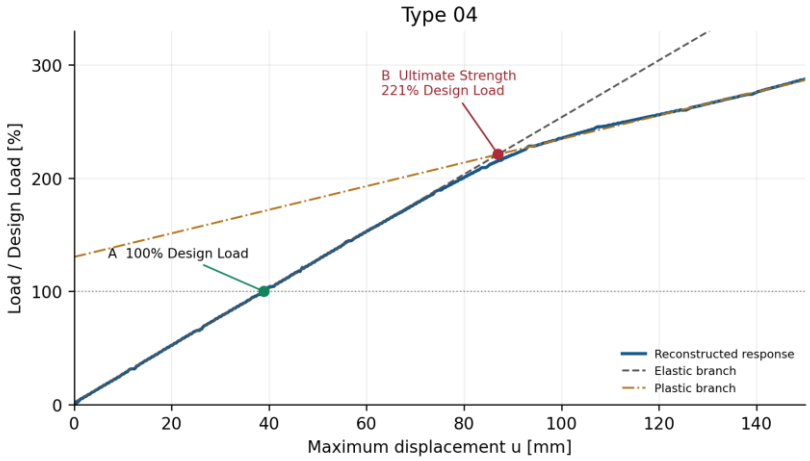


(b) Stress and displacement contours at A, 100 % Design Load

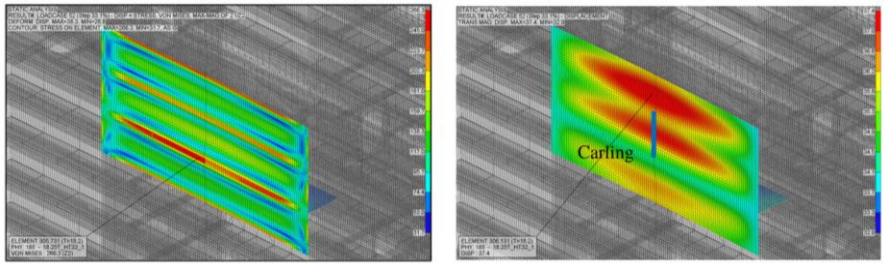


(c) Stress and displacement contours at B, Ultimate Strength

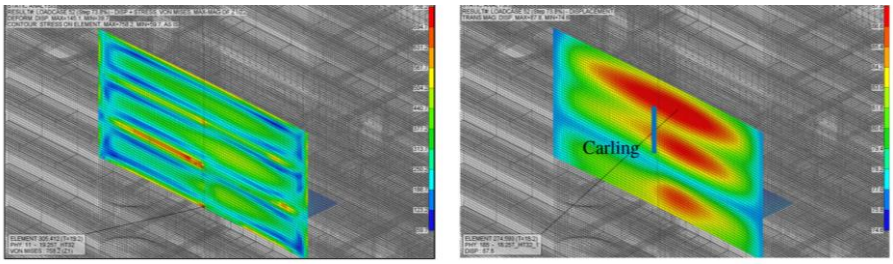
Fig. 14 Type 03 nonlinear response. A is 100 % Design Load and B is Ultimate Strength by the elastic and plastic branch intersection. The curve is a graphical reconstruction; the associated contours are retained from the supplied analysis



(a) Load displacement response with A at 100 % Design Load and B at Ultimate Strength



(b) Stress and displacement contours at A, 100% Design Load

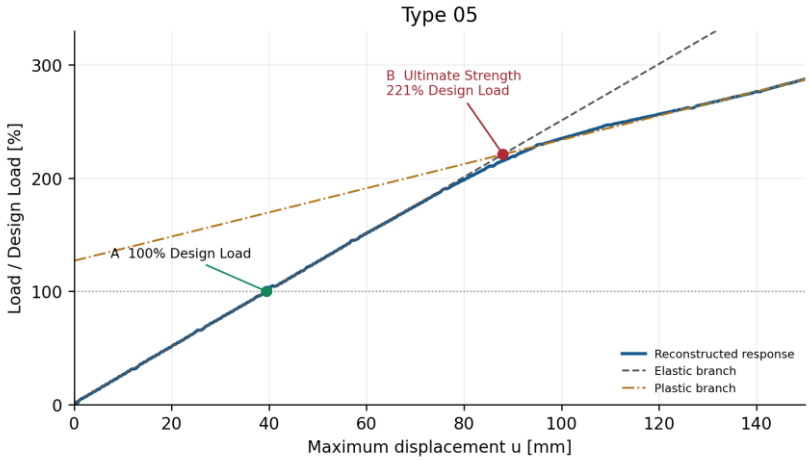


(c) Stress and displacement contours at B, Ultimate Strength

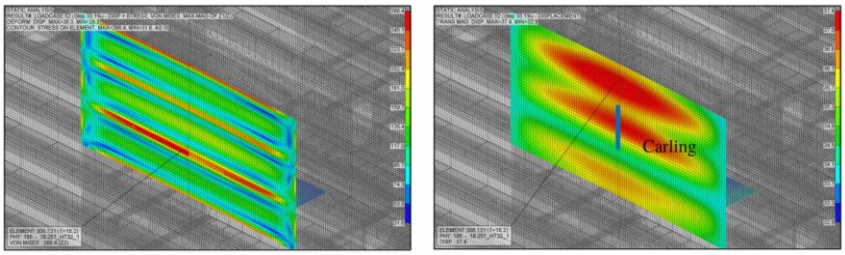
Fig. 15 Type 04 nonlinear response. A is 100 % Design Load and B is Ultimate Strength by the elastic and plastic branch intersection. The curve is a graphical reconstruction; the associated contours are retained from the supplied analysis

Type 04 shifts the single retained carling from 50 to 190 mm offset. The reported $\lambda_u = 2.21$ shows no strength penalty relative to Type 03 at the precision of the supplied results. The relevant feature is a local change in restraint position without a corresponding reduction in the overall nonlinear response. The small increase is not interpreted as a statistically established improvement.

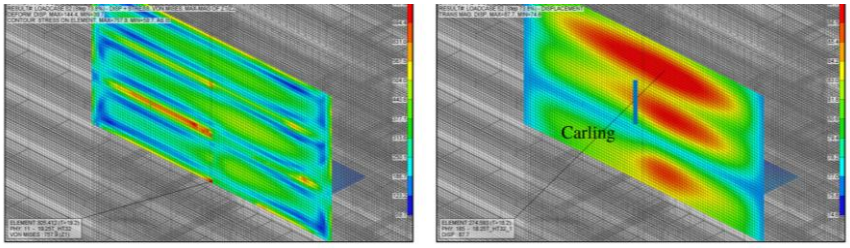
Type 05 extends the offset to 240 mm and retains $\lambda_u = 2.21$. Together with Type 04, it tests the upper part of the investigated offset range. The lack of a monotonic strength reduction supports offset insensitivity within this model and loading, while leaving effects on weld stress ranges, stiffener tripping and dynamic response outside the demonstrated scope.



(a) Load displacement response with A at 100 % Design Load and B at Ultimate Strength



(b) Stress and displacement contours at A, 100 % Design Load



(c) Stress and displacement contours at B, Ultimate Strength

Fig. 16 Type 05 nonlinear response. A is 100 % Design Load and B is Ultimate Strength by the elastic and plastic branch intersection. The curve is a graphical reconstruction; the associated contours are retained from the supplied analysis

3.5 Comparative summary

Table 8 compares Type 01 with Type 03 because these models most clearly represent the presence and absence of intermediate carling stiffeners between the ordinary stiffeners. Type 01 contains three aligned carlings, whereas Type 03 contains only one unwelded carling at a 50 mm offset. The linear stress and displacement differences remain small: Type 03 shows 1.7 % lower plate stress, 0.7 % lower stiffener stress, and 0.3 % higher displacement. In contrast, the first eigenvalue decreases from 1.397 to 1.316 (approximately 5.8 %) when the two intermediate carlings are removed. The nonlinear Ultimate Strength factor changes by only 0.5 %, from 2.20 to 2.19, showing that the intermediate carlings materially affect elastic bifurcation but do not govern the final load-carrying capacity of the panel.

Table 8 Representative comparison of Type 01 (three carlings) and Type 03 (single carling)

Quantity	Type 01	Type 03
Plate max. von Mises stress at DL [MPa]	194.9	191.5
Stiffener max. von Mises stress at DL [MPa]	300.7	298.7
Max. displacement at DL [mm]	102.3	102.6
First eigenvalue factor, λ_1 [–]	1.397	1.316
Ultimate Strength factor λu [× Design Load]	2.20	2.19

3.6 Ultimate strength at the design and tangent intersection states

Table 9 collects the nonlinear quantities at the two common states. A corresponds to 100 % Design Load, and B to Ultimate Strength defined in Equations (2) and (3). The factors λ_u span 2.19 to 2.21. Approximate displacements are retained from the original reporting; graphic redraws should not be used to infer additional numerical precision. The small differences indicate closely comparable computed strengths, rather than a resolved ranking once mesh, imperfection and fitting uncertainties are considered.

Table 9 Nonlinear response at the design-load point A and Ultimate Strength point B for Types 01-05

Model	A Design Load factor λ_A	Approx. displacement at A [mm]	B Ultimate Strength factor λ_u	Approx. displacement at B [mm]
Type 01	1.00	≈39	2.20	≈89
Type 02	1.00	≈39	2.19	≈86
Type 03	1.00	≈39	2.19	≈88
Type 04	1.00	≈38	2.21	≈87
Type 05	1.00	≈38	2.21	≈88

4. Discussion

4.1 Linear response equivalence

The close agreement of the design load membrane responses indicates that the unchanged plating and ordinary stiffeners dominate the reference stiffness. This explains why a moderate change in local carling restraint has little influence on A. These component membrane quantities should remain separate from the mesh dependent local peak stresses reported in the numerical verification section.

4.2 Relationship between eigenvalue buckling and nonlinear ultimate strength

Elastic buckling and the two tangent Ultimate Strength measure different aspects of response. The first is governed by the restraint of an admissible elastic mode; the second is determined by the change from high initial stiffness to the degraded stiffness branch of the imperfect panel. Carlings can therefore change the modal restraint without controlling the later redistribution through ordinary stiffeners and effective plating. This interpretation accounts for the different sensitivities observed here, but does not remove the need to assess imperfections and welding residual stress.

4.3 Practical implications for design and verification

For this bulkhead, the numerical results support examining a reduced carling detail when fabrication access requires it. The decision should consider design load response, elastic instability and Ultimate Strength together with fatigue and other applicable limit states. A nearly unchanged λu alone does not establish that a revised detail is acceptable under a different loading or tolerance condition.

4.4 Implications for fabrication sequencing and production cost

Removing two carlings may reduce handling, fit up, welding access conflicts and inspection effort. These are potential benefits, not measured outcomes. The cost illustration below uses the planning assumptions supplied with the manuscript; it is not a validated production dataset. Structural equivalence of an attachment without a shell weld is not established by the present models.

Types 03 to 05 each remove two parts and their associated intersection work. Because their computed Ultimate Strength factors remain close, the retained carling position may offer flexibility for fit up and welding access within the tested range. Section 4.4 translates this geometric opportunity into a planning cost estimate; it does not treat the small strength differences as an optimization ranking.

To express the production effect in economic terms, the cost of one carling was estimated from the planning norms of a large Korean shipyard (Table 10). Fillet welding of one carling to the shell plating requires 3.0 man-hours (M/H), valued at KRW 39,000 per M/H. The heat input to the thin shell plate causes angular and out-of-plane distortion, which is straightened at KRW 80,000 per M/H of shell welding, and it burns the coating on the opposite face, which is re-applied at KRW 40,000 per M/H. The weld also requires non-destructive testing (NDT), comprising preparation, inspection, and reporting, with 5.0 M/H per carling at the same labour rate. The cost of one carling is therefore $C_c = h_w \times (c_w + c_p + c_d) + h_n \times c_n$ = KRW 672,000, where h_w and h_n are the welding and NDT man-hours, c_w and c_n the corresponding labour rates, and c_p and c_d the coating and straightening costs per M/H of shell welding. Straightening and NDT account for 64.7 % of this cost and welding labor for only 17.4 %, so the cost of a shell weld is governed by the inspection and rework that follow it rather than by the weld itself.

Table 10 Cost of one carling fillet-welded to the shell plating, from shipyard planning norms (M/H = man-hour)

Cost item	Basis	Cost [KRW]	Share [%]
Welding to the shell plating	3.0 M/H × KRW 39,000	117,000	17.4
NDT (preparation, inspection, report)	5.0 M/H × KRW 39,000	195,000	29.0
Coating re-application (burn damage)	3.0 M/H × KRW 40,000	120,000	17.9
Straightening of distortion	3.0 M/H × KRW 80,000	240,000	35.7
Total per carling		**672,000**	**100.0**

If the retained carling is attached without a weld on the shell plating, the coating and straightening costs are avoided, and the welding and NDT man-hours change in proportion to the weld-length ratio φ of the new attachment relative to the baseline, taking man-hours as proportional to weld length. The saving per carling is KRW 360,000 (53.6 %) for $\varphi = 1.0$, when the same weld length is moved to non-shell members, KRW 516,000 (76.8 %) for $\varphi = 0.5$, and KRW 672,000 (100 %) for $\varphi = 0$ (Table 11). The cost of the alternative attachment is not included; its break-even value equals the saving.

Table 11 Saving per carling when the shell weld is avoided, for weld-length ratio φ of the proposed detail

Case	φ	Cost of proposed detail [KRW]	Saving [KRW]	Reduction [%]
Baseline (shell weld)	1.0 (on shell)	672,000	–	–
Case A: no weld	0	0	672,000	100.0
Case B: half weld length	0.5	156,000	516,000	76.8
Case C: same weld length, off shell	1.0	312,000	360,000	53.6

Table 12 applies these values to the five arrangements for the examined bay. Type 01 has three carlings and an estimated cost of KRW 2,016,000 per bay, comprising 9.0 M/H of welding and 15.0 M/H of NDT. Types 03-05 omit two carlings and thereby avoid 6.0 M/H of welding, 10.0 M/H of NDT, and the associated

rework, a saving of KRW 1,344,000 per bay (66.7 %) if the retained carling is attached as in Type 01. The offset of the retained carling is not assumed to change the man-hours, so the saving is the same for Types 03, 04, and 05. No cost saving is assigned to Type 02, which retains three carlings, because the reduction in weld length associated with the unwelded intersection was not quantified; furthermore, potential savings from fit-up and handling were excluded. If the retained carling is also installed without shell-side welding, the corresponding cost savings increase to KRW 1,704,000, KRW 1,860,000, and KRW 2,016,000 per bay, representing 84.5 %, 92.3 %, and 100 % of the maximum saving for φ = 1.0, 0.5, and 0, respectively. These additional savings are conditional. The finite element models of this study vary the connection between the carling and the ordinary stiffener, not between the carling and the shell plating, so the structural equivalence of a detail without a shell weld is not demonstrated here and must be verified separately.

Table 12 Estimated production cost and saving per bay for Types 01-05 (retained carling attached as in Type 01 unless stated)

Arrangement	Carlings per bay	Welding / NDT [M/H per bay]	Cost per bay [KRW]	Saving per bay [KRW]	Reduction [%]
Type 01	3	9.0 / 15.0	2,016,000	–	–
Type 02	3	9.0 / 15.0	2,016,000	0 (not credited)	0
Types 03-05, retained carling as in Type 01	1	3.0 / 5.0	672,000	1,344,000	66.7
Types 03-05, retained carling off shell, Case C (φ = 1.0)	1	3.0 / 5.0	312,000	1,704,000	84.5
Types 03-05, retained carling off shell, Case B (φ = 0.5)	1	1.5 / 2.5	156,000	1,860,000	92.3
Types 03-05, retained carling off shell, Case A (φ = 0)	1	0 / 0	0	2,016,000	100.0

The estimate is limited by the following points. The unit rates and the 3.0 and 5.0 M/H norms are planning values, not measured data, and vary with shipyard, plate thickness, and the NDT method specified. The NDT labour rate was assumed equal to the welding rate, and the coating and straightening costs were assumed to scale with the man-hours of shell welding. If no NDT is required for the welds that remain on non-shell members, the saving for φ = 1.0 increases from KRW 360,000 to KRW 555,000 per carling (82.6 %). Because the values are linear in the number of bays, a saving of KRW 1,344,000 per bay corresponds to KRW 134.4 million per 100 bays. Distortion, quality, and lead-time effects were not monetised. These estimates should therefore be regarded as a potential production benefit, to be confirmed by the shop-level trial described in Section 5.

4.5 Dependence on load combination

The observed response concerns lateral hydrostatic pressure combined with hull induced boundary deformation. Carlings may become important when stiffener tripping, in plane compression, shear buckling, cyclic stress or impact response governs. A new assessment is required for changes in load combination, boundary restraint, degradation or tolerances. Fatigue and dynamic adequacy cannot be inferred from the static Ultimate Strength assessment.

4.6 Influence of welding residual stress

Self-equilibrated welding residual stresses can cause earlier local yielding and modify load redistribution after buckling [2, 3, 13]. Their omission may overpredict resistance under compressive loading; neither the magnitude nor the sign of the correction for this combined load case has been quantified. Applying the same omission to all models does not prove that their ranking or a 0.5 % difference is insensitive to welding history. A residual stress sensitivity assessment remains necessary for absolute capacity claims.

5. Conclusions

Under the combined hydrostatic and hull deformation Design Load, reducing three carlings to one lowers the first elastic buckling factor from approximately 1.397 to 1.316, while Ultimate Strength by the two tangent method changes from 2.20 to 2.19 times Design Load. Across all five arrangements, λ_u remains between 2.19 and 2.21. The structural implication is that a local member may contribute to elastic modal restraint without governing the corresponding nonlinear redistribution capacity. A is consistently defined as 100 % Design Load and B as the elastic and plastic branch intersection throughout the study.

The four-mesh assessment establishes the intended scope of the 50 mm choice. Relative to 20 mm, it preserves reported linear displacement, changes the first eigenvalue by only 0.69 %, and reduces the whole sub model element count by 17.2 %. Similar nonlinear path shape and distributed deformation support its use for comparing carling arrangements. Higher load compliance shows finite sensitivity, including an approximate 6.4 % difference at the final common plotted ordinate, and the local stress maximum is unresolved. The mesh is therefore an effective engineering compromise for this panel study, not a universally optimal discretization or a local stress convergence claim. Verification of material and boundary records, imperfection mode, residual stress, fatigue and other load combinations remains necessary for absolute design acceptance. Fabrication savings based on planning assumptions require shop confirmation.

Future work should prioritize direct export of the nonlinear histories and common tangent fitting intervals to quantify mesh and Ultimate Strength uncertainty. Sensitivity studies should then vary imperfection mode and amplitude and introduce equilibrated welding residual stresses. Physical tests of the reference and reduced carling arrangements under combined pressure and membrane loading would provide independent validation. Additional compression, shear, fatigue, dynamic loading and corrosion cases are needed to establish the limits of the reduced detail. Finally, shop trials should measure weld length, fit up and inspection effort, distortion and production cost so that the estimated fabrication benefit can be evaluated against structural performance.

FUNDING

This work was supported by the Shipbuilding and Offshore Industry Core Technology Development Program (RS-2026-25620355) funded by the Ministry of Trade, Industry and Energy (MOTIE, Korea).

REFERENCES

[1] Lee, S., Kim, S., Kim, M., Oh, S., Stephens, A., 2020. Prelude hull cargo containment system. *Offshore Technology Conference*, 4-7 May, Houston, Texas, USA, OTC-30844-MS. https://doi.org/10.4043/30844-MS

[2] Paik, J. K., Thayamballi, A. K., 2003. Ultimate Limit State Design of Steel-Plated Structures. *John Wiley & Sons*, Chichester, UK.

[3] Paik, J. K., 2018. Ultimate Limit State Analysis and Design of Plated Structures, 2nd ed. *John Wiley & Sons*, Hoboken, NJ, USA. https://doi.org/10.1002/9781119367758

[4] Kim, D. K., Lim, H. L., Yu, S. Y., 2018. A technical review on ultimate strength prediction of stiffened panels in axial compression. *Ocean Engineering*, 170, 392-406. https://doi.org/10.1016/j.oceaneng.2018.10.022

[5] Anyfantis, K. N., 2020. Ultimate strength of stiffened panels subjected to non-uniform thrust. *International Journal of Naval Architecture and Ocean Engineering*, 12, 325-342. https://doi.org/10.1016/j.ijnaoe.2020.03.003

[6] Momčilović, N., Ilić, N., Kalajdžić, M., Ivošević, Š., Petrović, A., 2024. Effect of corrosion-induced structural degradation on the ultimate strength of a high-tensile-steel ship hull. *Journal of Marine Science and Engineering*, 12(5), 745. https://doi.org/10.3390/jmse12050745

[7] International Association of Classification Societies, 2024. UR S35: Buckling Strength Assessment of Ship Structural Elements, Corr.1. *IACS*, London, UK.

[8] American Bureau of Shipping, 2016. Guide for Buckling and Ultimate Strength Assessment for Offshore Structures, LRFD Version. *ABS*, Houston, Texas, USA.

[9] Lee, S. E., Thayamballi, A. K., Paik, J. K., 2015. Ultimate strength of steel brackets in ship structures. *Ocean Engineering*, 101, 182-200. https://doi.org/10.1016/j.oceaneng.2015.04.030

[10] Zhang, Q., Yang, H., Wu, S., Cheng, W., Liang, Y., Huang, Y., 2023. A study on the ultimate strength and failure mode of stiffened panels. *Journal of Marine Science and Engineering*, 11(6), 1214. https://doi.org/10.3390/jmse11061214

[11] Sholikhah, M., Ridwan, R., Prabowo, A. R., Ghanbari-Ghazijahani, T., Yaningsih, I., Muhayat, N., Tjahjana, D. D. D. P., Adiputra, R., Sohn, J. M., 2024. Strength assessment of stiffened-panel structures against buckling loads: FE benchmarking and analysis. *Civil Engineering Journal*, 10(4), 1034-1050. https://doi.org/10.28991/CEJ-2024-010-04-03

[12] Hanif, M. I., Adiputra, R., Prabowo, A. R., Yamada, Y., Firdaus, N., 2023. Assessment of the ultimate strength of stiffened panels of ships considering uncertainties in geometrical aspects: Finite element approach and simplified formula. *Ocean Engineering*, 286, 115522. https://doi.org/10.1016/j.oceaneng.2023.115522

[13] Li, S., Kim, D. K., Benson, S., 2021. The influence of residual stress on the ultimate strength of longitudinally compressed stiffened panels. *Ocean Engineering*, 231, 108839. https://doi.org/10.1016/j.oceaneng.2021.108839

[14] Park, J.-S., Yi, M.-S., 2024. Root causes of thin-plate buckling damage at the aft-end in crude oil tanker and verification through buckling analysis. *Metals*, 14(2), 158. https://doi.org/10.3390/met14020158

[15] Bahmani, M., Morshedsolouk, F., Khedmati, M. R., 2024. Effect of cracked and notched stiffeners on the ultimate strength of steel stiffened panels. *Journal of Marine Science and Application*, 23(2), 460-469. https://doi.org/10.1007/s11804-024-00417-2

[16] Silva-Campillo, A., Ulla-Campos, L., Suárez-Bermejo, J. C., Herreros-Sierra, M. A., 2022. Effect of bow hull form on the buckling strength assessment of the corner bracket connection. *Ocean Engineering*, 265, 112562. https://doi.org/10.1016/j.oceaneng.2022.112562

[17] Vu, V. T., Do, Q. T., Doan, V. T., Cu, H. C., Vu, T. A., 2026. Numerical study of bottom stiffened panels under combined loading with initial imperfections and uniform corrosion. *Journal of Ocean Engineering and Marine Energy*, 12, 1139-1149. https://doi.org/10.1007/s40722-026-00479-0

[18] Saad-Eldeen, S., Garbatov, Y., 2023. Experimental and numerical analysis of structural capacity of perforated stiffened plates. *Journal of Marine Science and Engineering*, 11(4), 842. https://doi.org/10.3390/jmse11040842

[19] Fhandy, B. A., Prabowo, A. R., Tuswan, T., Zubaydi, A., Smaradhana, D. F., Baek, S. J., Fitri, S. N., 2025. Crashworthiness behaviour of the stiffened panel in idealized penetration test: A developed stiffening configuration against impact loading. *Brodogradnja*, 76(2), 76205. https://doi.org/10.21278/brod76205

[20] Tu, J., Feng, F., Lu, Y., Wang, S., Cao, Q., 2025. Structural strength evaluation of a planing hull based on a one-way coupled CFD-FEA. *Brodogradnja*, 76(4), 76407. https://doi.org/10.21278/brod76407

[21] Lee, G. N., Jung, K. H., 2026. Assessment of pressure-time-based wave impact criteria from a structural response perspective: Application to green water loads. *Brodogradnja*, 77(4), 77404. https://doi.org/10.21278/brod77404

[22] Rognoni, G., Brocco, E., D'Amore, K.O., G., Biot, M., 2026. Low-frequency structural vibration reduction in stiffened panels using integrated acoustic black holes. *Brodogradnja*, 77(4), 77408. https://doi.org/10.21278/brod77408

[23] Jeong, D., Kim, D., Choi, T., Seo, Y., 2020. A process-based modeling method for describing production processes of ship block assembly planning. *Processes*, 8(7), 880. https://doi.org/10.3390/pr8070880

[24] Det Norske Veritas, 2013. DNV-RP-C208: Determination of Structural Capacity by Non-linear FE Analysis Methods. June 2013. *DNV*, Høvik, Norway.